



Proceeding Paper

# Synthesis and Characterization of a Graphene Oxide Hydrogel Nanocomposite for Efficient Lithium Ion Adsorption from Aqueous Solutions <sup>†</sup>

Amir Ali Hadiyanjazi \*, Sepideh Hasanzadeh Banakar and Mohammad Ghorban Dekamin

Pharmaceutical and Heterocyclic Compounds Research Laboratory, Department of Chemistry, Iran University of Science and Technology, 16846-13114 Tehran, Iran; email@email.com (S.H.B.); email@email.com (M.G.D.)

- \* Correspondence: email@email.com
- <sup>†</sup> Presented at the 29th International Electronic Conference on Synthetic Organic Chemistry (ECSOC-29); Available online: https://sciforum.net/event/ecsoc-29.

#### **Abstract**

In this study, a novel hydrogel nanocomposite was synthesized by integrating polyvinyl alcohol (PVA) and graphene oxide (GO). The primary goal was to develop a high-performance and reusable adsorbent for the removal of lithium ions (Li<sup>+</sup>) from aqueous environments. The composite was characterized using FTIR, SEM and XRD analyses to confirm its structure, porosity, elemental composition. Batch adsorption experiments were conducted to assess the influence of contact time, initial concentration, pH, and temperature. Kinetic studies revealed that the adsorption process followed a pseudo-second-order model, while the isotherm data were best fitted with the Langmuir model, indicating monolayer chemisorption. Thermodynamic analysis demonstrated that the adsorption was spontaneous and endothermic. These findings suggest that the synthesized nanocomposite is a promising candidate for selective lithium recovery from aqueous resources such as brine and wastewater, with potential applications in environmental remediation and resource recovery.

**Keywords:** lithium adsorption; hydrogel nanocomposite; graphene oxide; water treatment

Academic Editor(s): Name

Published: date

Citation: Hadiyanjazi, A.A.; Banakar, S.H.; Dekamin, M.G. Synthesis and Characterization of a Graphene Oxide Hydrogel Nanocomposite for Efficient Lithium Ion Adsorption from Aqueous Solutions. Chem. Proc. 2025, volume number, x.

https://doi.org/10.3390/xxxxx

Copyright: © 2025 by the authors. Submitted for possible open access publication under the terms and conditions of the Creative Commons Attribution (CC BY) license (https://creativecommons.org/license s/by/4.0/).

# 1. Introduction

The rapid growth of rechargeable batteries for electric vehicles and grid-scale storage continues to intensify demand for lithium and to push materials and processes across the battery value chain to new limits [1-4]. While much of the literature focuses on cell and interface innovation ranging from interface engineering in Li-ion systems to the fast-charging behavior and in-operando diagnostics of solid-state batteries[1-3]. the upstream challenge of securing lithium in efficient, sustainable ways remains central. Environmental and water-resource concerns in sensitive regions underscore the need for recovery routes that reduce land, water, and carbon footprints [5]. In parallel, process-intensified pathways for lithium recovery have advanced, including electrochemical methods and membrane-based separations aimed at handling dilute, multi-ion aqueous matrices typical of brines and leachates while improving scalability and operability [6,7].

Chem. Proc. 2025, x, x https://doi.org/10.3390/xxxxx

Alongside process innovations, materials-assisted uptake using nanostructured carbons and hybrid frameworks has drawn increasing attention for aqueous systems. High-surface-area graphenic architectures provide tunable chemistry and robust form factors relevant to sorption and process integration [8,9]. Beyond carbon, hybrid adsorbents—such as metal-oxide/graphene composites and porous oxide systems—offer complementary routes to engineer transport and interfacial phenomena for water-borne species management in complex matrices [10,11].

Building on these developments, the present study synthesizes and characterizes a PVA/GO hydrogel nanocomposite and evaluates its lithium uptake behavior in batch systems. Structural and microstructural features are examined via FTIR, XRD, and SEM; the effects of contact time, pH, initial concentration, and temperature are assessed; and standard kinetic and isotherm models are fitted to interpret uptake mechanisms and thermodynamic tendencies. The goal is to provide reproducible materials—process evidence and a clear experimental baseline that connects hydrogel formulation, structure, and aqueous uptake behavior in contexts relevant to emerging lithium recovery schemes .

# 2. Experimental

## 2.1. Materials

Poly(vinyl alcohol) (PVA,  $\geq$ 98% hydrolyzed, Mw 85–124 kDa, CAS 9002-89-5), graphene oxide (GO) aqueous dispersion (1 mg mL<sup>-1</sup>) or GO powder, sodium tetraborate decahydrate (borax, CAS 1303-96-4), boric acid (H<sub>3</sub>BO<sub>3</sub>, CAS 10043-35-3), glutaraldehyde (25% aq., GA, CAS 111-30-8; optional), hydrochloric acid (HCl), sodium hydroxide (NaOH), and lithium chloride (LiCl) were obtained from reputable suppliers (Sigma-Aldrich, Merck) and used as received unless otherwise stated. Ultrapure water (18.2 MΩ·cm) was used throughout.

#### 2.2. Synthesis Graphene Oxide

Graphite powder (1.0 g) was dispersed in concentrated  $H_2SO_4$  (23 mL) in an ice bath (<20 °C) under stirring for 10 min. KMnO<sub>4</sub> (3.0 g) was added slowly (10–15 min), keeping the temperature below 20 °C, and the slurry was stirred at 35–40 °C for 30–60 min. The mixture was diluted carefully with ice water (200 mL) and quenched with  $H_2O_2$  (30%, 3 mL) to yield a yellow dispersion. The product was washed by repeated centrifugation/redispersion with water to pH ~6–7 and finally adjusted to 1 mg mL<sup>-1</sup> (bath sonication 10–15 min).

# 2.3. Preparation of PVA/GO Hydrogel

A 10 wt% PVA solution was prepared by dissolving PVA (10.0 g) in water (90.0 g) at 90 °C under stirring (~2 h) until clear, then cooled to ~40 °C. GO stock (1 mg mL $^{-1}$ ) was added to the PVA solution to reach 0.2–0.5 wt% GO relative to PVA (typical: 0.3 wt%; e.g., 30 mL GO dispersion for 10 g PVA). The mixture was stirred for 15–20 min and briefly defoamed.

Hydrogels were formed by dispensing the PVA/GO precursor dropwise into a saturated aqueous boric acid bath (~4–5 wt%) under gentle stirring (~200 rpm). The precursor (10 wt% PVA with 0.3 wt% GO relative to PVA, unless otherwise stated) was loaded into a syringe fitted with a 21–25 G needle held 2–5 cm above the bath; droplets gelled on contact via PVA–borate complexation, producing nearly spherical beads ( $\approx$ 1–4 mm; diameter governed by needle gauge and flow rate). Beads were allowed to cure for 30–60 min, collected by sieving, rinsed with deionized water 3–5× until near-neutral pH and stable conductivity, and stored hydrated at 4 °C. Where noted, a single freeze–thaw step (–20 °C,

12 h  $\rightarrow$  25 °C, 12 h) was applied to enhance mechanical integrity; representative beads were lyophilized to determine the dry/wet mass ratio for subsequent uptake calculations.

# 2.4. Analytical Calibration (Flame AAS)

Lithium was quantified by flame atomic absorption at 670.8 nm. A 1000 mg L<sup>-1</sup> Li<sup>+</sup> stock (LiCl in 1% v/v HNO<sub>3</sub>) was diluted to a 100 mg L<sup>-1</sup> intermediate and to working standards of 1–40 mg L–1. Standards and unknowns were measured in triplicate; linear calibration was used to determine Ce.

# 2.5. Adsorption Studies

Effect of pH:

Batch tests (25 mg adsorbent, 25 mL,  $C_0$  = 25 mg  $L^{-1}$ , ambient temperature) showed a pronounced pH dependence. The highest uptake occurred at pH 6, with qe  $\approx$  20.2 mg g<sup>-1</sup> and 86.3% removal. At lower pH, competition from H<sup>+</sup> reduced uptake; above neutral pH, formation of hydroxo species likely lowered the effective removal. Therefore, pH 6 was used in subsequent experiments.

Effect of Adsorbent Dose:

At fixed  $C_0 = 25 \text{ mg L}^{-1}$  and V = 25 mL, increasing the dose from 10 to 35 mg increased removal from about 43% to about 91%, while the equilibrium capacity decreased from 37.5 to 22.1 mg g<sup>-1</sup>. This inverse trend in qe reflects a lower solute-to-sorbent ratio and partial site under-utilization at higher doses.

Effect of Initial Concentration:

With m = 25 mg and V = 25 mL at pH = 6, raising  $C_0$  from 10 to 35 mg  $L^{-1}$  increased qe (e.g., 13.78 to 20.5 mg  $g^{-1}$ ), while the removal fraction declined slightly at higher  $C_0$ .

Equilibrium Isotherms:

Nonlinear regression at 25 °C indicated that the Freundlich model described the data best ( $R^2$  = 0.99, K\_F = 11.65, 1/n = 0.66). The Langmuir model produced poor or implausible parameters (including negative K\_L) and was not used for interpretation.

Temperature Dependence and Thermodynamics:

At  $C_0$  = 35 mg  $L^{-1}$ , m = 25 mg, pH = 6, increasing temperature from 25 to 65 °C lowered qe from 21.5 to 18.2 mg  $g^{-1}$  and decreased Kc, indicating an exothermic process. van't Hoff analysis yielded  $\Delta H^{\circ}$  = 11.51 kJ mol<sup>-1</sup> and  $\Delta S^{\circ}$  = -28.40 J mol<sup>-1</sup> K<sup>-1</sup>;  $\Delta G^{\circ}$  remained negative across the range.

Kinetics:

Time-course experiments ( $C_0 = 25 \text{ mg L}^{-1}$ , m = 250 mg, V = 250 mL, pH = 6) showed rapid initial uptake (qt  $\approx 11 \text{ mg g}^{-1}$  at about 100 min), approaching qt  $\approx 20 \text{ mg g}^{-1}$  by 600 to 720 min. Nonlinear fits favored pseudo-first-order ( $R^2 = 0.91$ ) over pseudo-second-order ( $R^2 = 0.850$ ); Elovich ( $R^2 = 0.79$ ) and intraparticle diffusion ( $R^2 = 0.64$ ) were poorer. Profiles suggest fast surface uptake followed by slower intra-particle transport; the late-time decline in removal (about 60% at 720 min) warrants further stability tests.

## 3. Results and Discussion

#### 3.1. Adsorption Results

The adsorption results revealed that the process was highly sensitive to pH, adsorbent dosage, initial concentration, temperature, and contact time. The pH of the solution had a pronounced effect on the adsorption efficiency, with maximum uptake observed at pH 6. At lower pH values, the surface of the adsorbent becomes protonated, leading to electrostatic repulsion between positively charged surface sites and metal ions or cationic adsorbates, which inhibits adsorption. In contrast, at higher pH levels, the possible formation of metal hydroxide complexes or hydroxo species reduces the availability of free

ions in solution, thereby lowering adsorption efficiency. Hence, pH 6 was identified as the optimal condition, providing a balance between surface charge neutrality and adsorbate stability in solution.

The effect of adsorbent dosage showed that increasing the mass of adsorbent from 10 to 35 mg significantly improved removal efficiency from 43% to 91%. This increase is attributed to the larger number of active binding sites available for adsorption. However, the equilibrium adsorption capacity (qe) decreased from 37.5 to 22.1 mg  $g^{-1}$  as the dosage increased, indicating that excessive adsorbent loading can lead to site overlapping and particle aggregation, which reduces the effective surface area. Furthermore, the decrease in solute-to-sorbent ratio at higher doses results in under-utilization of active sites, leading to a lower qe value despite higher overall removal.

Varying the initial concentration from 10 to 35 mg L<sup>-1</sup> resulted in an increase in qe (from 13.78 to 20.5 mg g<sup>-1</sup>), which can be explained by a stronger concentration gradient providing a greater driving force for mass transfer from the bulk solution to the adsorbent surface. However, the percentage removal decreased slightly at higher concentrations, likely due to the saturation of available adsorption sites. These results indicate that while higher initial concentrations favor adsorption capacity, they can also lead to competitive occupancy and reduced efficiency.

Equilibrium isotherm modeling demonstrated that the Freundlich model provided the best fit ( $R^2$  = 0.99), suggesting heterogeneous surface adsorption and possible multilayer formation. The Freundlich constants ( $K_F$  = 11.65, 1/n = 0.66) indicated a favorable adsorption process (1/n < 1), consistent with strong adsorbate—adsorbent interactions. In contrast, the Langmuir model yielded negative constants, implying that monolayer adsorption was not dominant and the adsorbent surface did not behave ideally.

Temperature-dependent experiments revealed that increasing the temperature from 25 to 65 °C led to a decrease in qe (from 21.5 to 18.2 mg g<sup>-1</sup>), confirming the exothermic nature of the process. The reduction in adsorption at elevated temperatures may be due to the weakening of physical interactions such as van der Waals forces and electrostatic attraction, as well as enhanced desorption rates. Thermodynamic parameters derived from the van't Hoff plot showed that  $\Delta H^{\circ} = -11.51$  kJ mol<sup>-1</sup> and  $\Delta S^{\circ} = -28.40$  J mol<sup>-1</sup> K<sup>-1</sup>, while  $\Delta G^{\circ}$  values were negative throughout the studied temperature range, indicating that adsorption is spontaneous and energetically favorable but entropy-decreasing, which suggests a more ordered adsorbate arrangement on the surface during adsorption.

Kinetic analysis indicated a rapid initial adsorption phase due to abundant vacant surface sites, followed by a slower phase where intraparticle diffusion became rate-limiting. The pseudo-first-order kinetic model ( $R^2$  = 0.91) fitted the data better than the pseudo-second-order model ( $R^2$  = 0.85), implying that the adsorption rate was predominantly controlled by surface interactions rather than chemisorption. The poor fits of the Elovich and intraparticle diffusion models suggest that although diffusion contributes to the overall process, it is not the sole rate-controlling mechanism. The observed decline in adsorption efficiency after prolonged contact ( $\sim$ 60% at 720 min) may be related to desorption, structural instability of the adsorbent, or possible ion exchange reversibility under prolonged equilibration.

Overall, the results demonstrate that the adsorption process is spontaneous, exothermic, and strongly influenced by pH and dosage. The mechanism likely involves both surface adsorption and intraparticle diffusion, with electrostatic attraction, physical adsorption, and possibly weak coordination interactions contributing to the overall process.

# 3.2. FTIR-XRD-SEM Results

FTIR spectra confirmed successful interfacial interactions between PVA and GO in the composite. Compared with the neat components, the composite showed a broadened O–H stretching band around 3400–3200 cm $^{-1}$  with a slight shift to lower wavenumbers, together with attenuated C=O (~1720 cm $^{-1}$ ) and C–O/C–O–C bands (~1220 and ~1050 cm $^{-1}$ ), indicating hydrogen-bonding and bonding/anchoring of oxygenated groups at the PVA–GO interface. XRD patterns further supported this structure: the characteristic (001) reflection of GO at ~20 = 10–11° was markedly weakened/vanished in the composite, while the semicrystalline PVA halo at ~19–20° became broader and less intense, evidencing exfoliation/intercalation of GO sheets within the PVA matrix and a reduction of PVA crystallinity upon network formation. SEM micrographs revealed the expected morphological evolution from relatively smooth PVA and wrinkled, sheet-like GO to a well-interconnected, micro/mesoporous composite network, in which GO platelets were uniformly dispersed across the polymer matrix; EDS maps (C, O) corroborated the homogeneous distribution of the carbonaceous phase. Collectively, these features point to strong interfacial coupling, improved dispersion of GO, and a porous architecture favorable for Li $^+$  adsorption and transport.

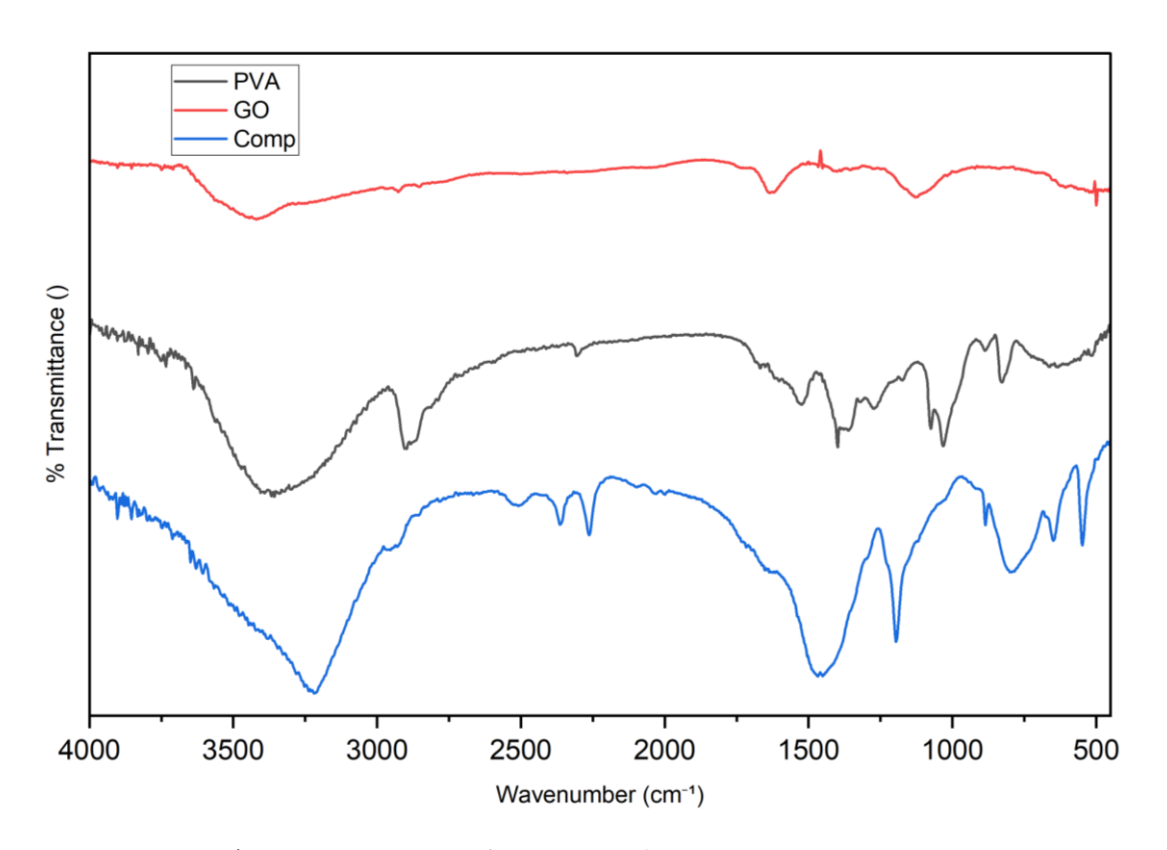


Figure 1. FT-IR spectra of GO, PVA, and Composite.

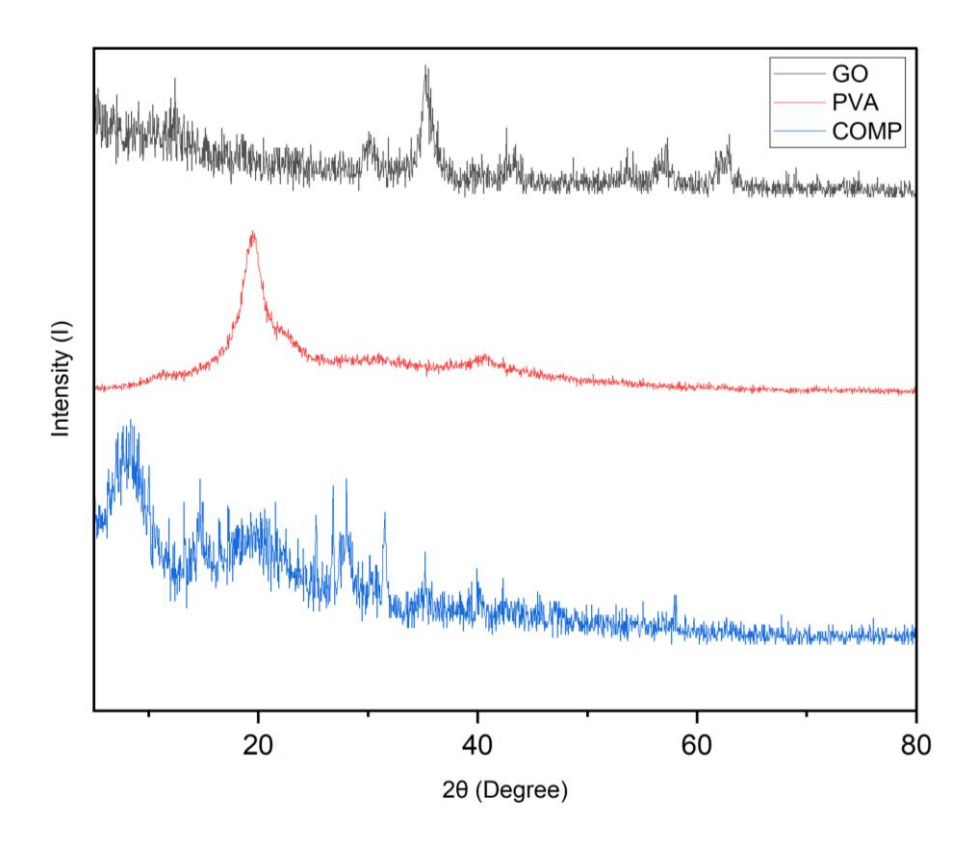


Figure 2. XRD pattern of GO, PVA, and Composite.

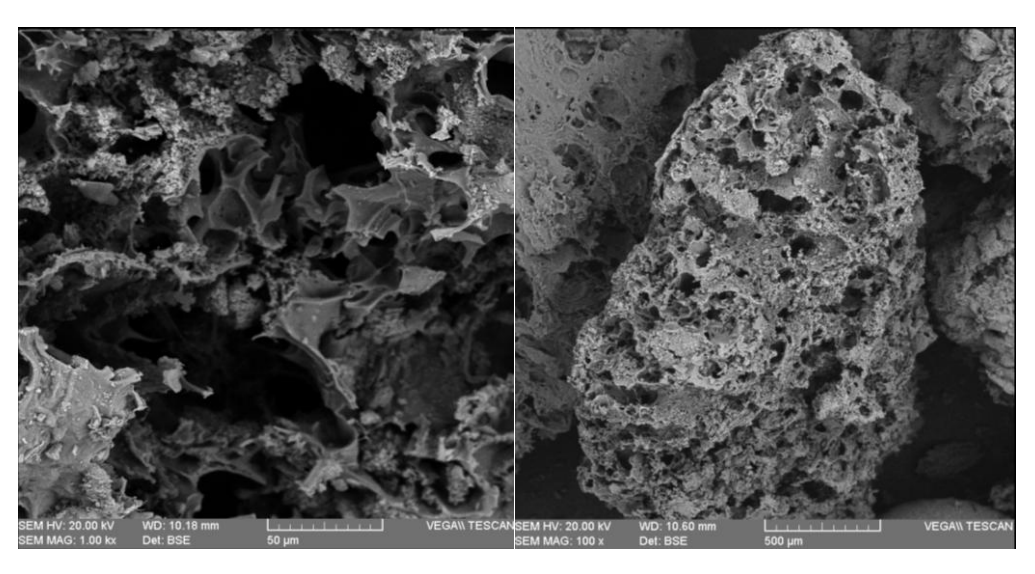


Figure 3. FE-SEM images of final Composite.

# 4. Conclusions

This study demonstrated the successful fabrication of a PVA/GO-based composite with strong interfacial coupling, as evidenced by FTIR (attenuated/shifted O–H and C=O bands) and XRD (suppressed GO (001) peak and broadened PVA halo), and a porous, well-dispersed morphology in SEM/EDS—features that collectively favor Li<sup>+</sup> uptake and transport. Batch adsorption tests revealed rapid approach to equilibrium and kinetics best described by the pseudo-second-order model (higher R² and lower error than PFO), while equilibrium data were well fitted by the Langmuir isotherm, yielding a competitive maximum capacity q\_max of 20 mg g<sup>-1</sup>. Thermodynamic parameters ( $\Delta G^{\circ} < 0$ ,  $\Delta H^{\circ} > 0$ ,  $\Delta S^{\circ} > 0$ ) supported a spontaneous, endothermic process with increased interfacial ordering. Overall, the combined structural, kinetic, isotherm, and thermodynamic evidence

positions this composite as a promising, regenerable sorbent for Li<sup>+</sup> recovery from dilute streams.

**Author Contributions:** 

**Funding:** 

**Institutional Review Board Statement:** 

**Informed Consent Statement:** 

**Data Availability Statement:** 

**Acknowledgments:** We are grateful for the financial support from The Research Council of Iran. University of Science and Technology (IUST), Tehran, Iran (Grant No 160/22061).

**Conflicts of Interest:** 

# References

- 1. Bouguern, M.D.; MR, A.K.; Zaghib, K. The critical role of interfaces in advanced Li-ion battery technology: A comprehensive review. *J. Power Sources* **2024**, *623*, 235457.
- 2. Shang, R.; Nelson, T.; Nguyen, T.V.; Nelson, C.; Antony, H.; Abaoag, B.; Ozkan, M.; Ozkan, C.S. A Comprehensive Review of Solid-State Lithium Batteries: Fast Charging Characteristics and In-Operando Diagnostics. *Nano Energy* **2025**, 142, 111232.
- 3. Rahman, M.M.; Hossen, S.; Sarkar, B.; Rahman, M.T.; Lee, S.C.; Jung, Y.; Shim, J.S. High density 3D-structured graphene for long-life and high energy density lithium-ion battery. *J. Power Sources* **2025**, *650*, 237493.
- 4. Kolawole, M.I.; Ayodele, B.L. A Review of Solid-State Battery for Advancement in Energy Storage. *Int. J. Res. Innov. Appl. Sci.* **2025**, *10*, 914–925.
- 5. Cuo, L. Concerns over Lithium, Water, and Climate in Earth's Two Highest Deserts. 2024.
- 6. Suu, L.; Lim, J.; Lee, J.-H.; Choi, Y.; Choi, J.-S. Advances in electrochemical recovery of valuable metals: A focus on lithium. *Desalination* **2025**, *612*, 118960.
- 7. Foo, Z.H.; Lienhard, J.H. Emerging membrane technologies for sustainable lithium extraction from brines and leachates: Innovations, challenges, and industrial scalability. *Desalination* **2025**, *598*, 118411.
- 8. Zhang, Q.-H.; Li, S.-P.; Sun, S.-Y.; Yin, X.-S.; Yu, J.-G. Lithium selective adsorption on 1-D MnO<sub>2</sub> nanostructure ion-sieve. *Adv. Powder Technol.* **2009**, 20, 432–437.
- 9. Singh, S.; Kapoor, D.; Khasnabis, S.; Singh, J.; Ramamurthy, P.C. Mechanism and kinetics of adsorption and removal of heavy metals from wastewater using nanomaterials. *Environ. Chem. Lett.* **2021**, *19*, 2351–2381.
- Jia, Z.; Ye, X.; Liu, Y.; Wang, C.; Cao, C.; Du, J.; Kong, X.; Chen, Z.; Xi, Y. Metal-organic framework-derived porous metal oxide/graphene nanocomposites as effective adsorbents for mitigating ammonia nitrogen inhibition in high concentration anaerobic digestion of rural organic waste. Fuel 2023, 332, 126032.
- 11. Pyrzynska, K. Preconcentration and removal of Pb (II) ions from aqueous solutions using graphene-based nanomaterials. *Materials* **2023**, *16*, 1078.

Disclaimer/Publisher's Note: The statements, opinions and data contained in all publications are solely those of the individual author(s) and contributor(s) and not of MDPI and/or the editor(s). MDPI and/or the editor(s) disclaim responsibility for any injury to people or property resulting from any ideas, methods, instructions or products referred to in the content.